SLAC–PUB–6706
December 1994
(A)

MAGNET ALIGNMENT TOLERANCES IN THE SLC FINAL FOCUS SYSTEM DETERMINED BY LIE ALGEBRA TECHNIQUES*

Frank Zimmermann◇

Stanford Linear Accelerator Center
Stanford University, Stanford, CA 94309

Abstract

Using Lie algebra techniques, static alignment tolerances are derived for all quadrupole and sextupole magnets in the 1994 SLC final focus. Three different effects are identified which limit the tolerable quadrupole misalignment. The largest amplitude of an offset-compensating closed orbit bump and the maximum allowed displacement between beam orbit and magnet center are evaluated for each sextupole. Multiparticle tracking supplements and confirms the analytical results.

Submitted to *Nuclear Instruments and Methods*

*Work supported by Department of Energy contract DE–AC03–76SF00515.

1 Introduction

1.1 The SLC Final Focus System

The final focus system of the Stanford Linear Collider (SLC) consists of two telescopes, Upper and Final Transformer (abbreviated in the following as UT and FT), separated by a Chromatic Correction Section (CCS) that accommodates two interleaved $-I$ sextupole pairs [1, 2, 3]. For convenience, we denote the sextupoles by $s0, s1, s2$ and $s3$, in the order of their position. The pair $(s0, s2)$ is used to control the horizontal chromaticity; the second pair $(s1, s3)$ compensates the vertical chromaticity. The $-I$ separation between the two sextupoles of each pair ensures that no third-order geometric aberrations are generated. However, the interleaved scheme gives rise to fourth-order terms, which will play a role in the tolerance analysis. In 1994, an upgrade to the SLC final focus system was installed to cancel the most important of the residual aberrations, and thereby to reduce the vertical spot size at the Interaction Point (IP) by a factor of two [4]. At low current, the expected spot size of about 450 nm is now routinely established.

In the case of an ideal alignment, the minimum spot size (as determined by tracking with MAD [5]) is obtained for $\beta_{x0} \approx 9$ mm and $\beta_{y0} \approx 1.4$ mm. For emittances of $\epsilon_x = 600$ μm μrad and $\epsilon_y = 60$ μm μrad, this corresponds to an rms-value of the horizontal and vertical divergence of $\theta_{x0} \approx 260\,\mu$rad and $\theta_{y0} \approx 204\,\mu$rad. The subindex '0' denotes values at the IP. Taking into account the effect (which is not chromatically corrected) of synchrotron radiation in the last three bending magnets (two inside and one behind the CCS), the beam sizes obtained from simulations are $\sigma_{y0} \approx 450$ nm and $\sigma_{x0} \approx 2.4$ μm, in agreement with the measurements.

1.2 The Lie Algebra Approach

Lie algebra techniques have been described in detail by Irwin [6]. Therefore, we only quote the main ideas used in the following tolerance analysis. The linear design optics between two locations of an arbitrary beam line can be characterized by a 4×4– or 6×6–dimensional transfer matrix, the so-called R–matrix [7, 8]. In the Lie algebra approach, the nonlinear deviation of a beam line M from the linear optics is written as a succession of nonlinear elements

$$\begin{aligned} M \;\;=\;\; \ldots\; & \exp\{-H_i(x_i, p_{xi}, y_i, p_{yi}, \delta)\} \\ & \exp\{-H_j(x_j, p_{xj}, y_j, p_{yj}, \delta)\} \\ & \exp\{-H_k(x_k, p_{xk}, y_k, p_{yk}, \delta)\}\ \ldots\ , \end{aligned} \tag{1.1}$$

where the Hamiltonians H_m in the exponents are typically polynomials of order three or four, and the arguments $x_m, p_{xm}, \ldots$ are the local coordinates and momenta at the center of the element described by the Hamiltonian H_m. As an example, the Hamiltonian of a sextupole magnet of integrated strength K_s is to a good approximation given by

$$H_s(x_s, p_{xs}, y_s, p_{ys}, \delta) \;=\; \frac{1}{6}\, K_s(x_s^3 - 3x_s\, y_s^2)\ . \tag{1.2}$$

Again, the subindex 's' indicates coordinates at the center of the sextupole. In Eq. (1.1), we have introduced the variable $\delta \equiv (\Delta p/p_0)\,/\,\{1 + (\Delta p/p_0)\}$, p_0 being the design momentum [6]. Note that, unlike Ref. [6], we do not use the colon ':' to indicate Lie generators. In this paper every expression that appears in an exponent is implicitly understood to be a Lie generator. Now, to determine the effect of the nonlinearities on the IP spot size, the operator M has to be applied to the coordinates at the IP. For that purpose, the local coordinates $x_i, p_{xi}, \ldots$ are translated into IP coordinates via the inverse 4×4 or 6×6 R–matrices

$$\vec{x}_i \;=\; R_{i\to 0}^{-1}\, \vec{x}_0 \;, \tag{1.3}$$

using the abbreviation $\vec{x} \equiv (x, p_x, y, p_y, \delta)$. Similarity transformations [6], i.e.,

$$e^A \cdot e^B \cdot e^{-A} \;=\; e^C \;, \quad \text{where} \quad C \;\equiv\; e^A B \;, \tag{1.4}$$

and the Baker–Campbell–Hausdorff theorem [6],

$$e^A e^B \;=\; e^{A+B+\;[A,B]/2\;+\;\cdots} \;, \tag{1.5}$$

allow an approximate expression of the series M, Eq. (1.1), in terms of a total nonlinear Hamiltonian

$$M \;\approx\; \exp\{-H_{\rm tot}(x_0, p_{x0}, y_0, p_{y0}, \delta)\} \;. \tag{1.6}$$

The nonlinear problem is then reduced to computing the Hamiltonian $H_{\rm tot}$ and evaluating its effect on the beam distribution at the IP. Later in this report, the Hamiltonian $H_{\rm tot}$ is calculated for several specific examples. The change of the vertical coordinate y_0 at the IP is

$$\Delta y_0 \;=\; [-H_{\rm tot}, y_0] \;+\frac{1}{2}\left[H_{\rm tot},\, [H_{\rm tot}, y_0]\right] + \;\ldots\; , \tag{1.7}$$

$$\approx\; \frac{\partial H_{tot,0}}{\partial p_{y0}} \;, \tag{1.8}$$

where the contribution from higher-order Poisson brackets can almost always be neglected. The increase of the rms value of the vertical spot size is given by

$$\Delta\sigma_{y_0}^2 \;\approx\; \left\langle (\Delta y_0)^2 \right\rangle - \langle \Delta y_0 \rangle^2 \,. \tag{1.9}$$

In Eq. (1.9), the angle-brackets denote an average over the (initial) bunch distribution, linearly propagated to the IP. It is often reasonable to assume that the initial distribution at the entrance of the final focus is Gaussian, in which case higher order moments in Eq. (1.9) are nicely reduced to powers of second-order moments. It should, however, be mentioned that the value for the vertical rms beam size given by Eq. (1.9), though exact, does not directly reflect the expected luminosity, because the beam shape at the IP is generally non-Gaussian, due to nonlinear aberrations in the final focus and also due to disruption [9].

2 Tolerance Criterion

In this report, we want to calculate the *static* alignment tolerances of quadrupole and sextupole magnets. These tolerances are due to the beam size increases that remain when all possible tuning algorithms, such as orbit correction, dispersion and chromaticity correction, waist shift, decoupling, etc., have been applied (see also Roy [10]). If these tolerance conditions are violated, the only possible cure is an actual movement of magnets. Other tolerances, such as those for vibrations or power supply jitter, refer to different, shorter time scales. Since over these time scales, less tuning and corrections can be performed, they are tighter than the static tolerances.

Guided by references [10, 11], the tolerances are deduced from the following criterion. We would like to allow for, at most, a 2% increase of the vertical spot size from each effect under consideration (such as horizontal or vertical displacement of quadrupole magnets, horizontal or vertical sextupole alignment, and so on). As is readily seen, this gives an upper limit on the increase of the square of the beam size of

$$\Delta\sigma^2_{y0,\mathrm{pert}} < 0.04\,\sigma^2_{y0} \tag{2.10}$$

for each individual effect. The motivation for this approach is that, in total, there may be about 5 to 7 effects contributing to the vertical spot size, which then result in an overall beam size increase of about 10 to 15% . This is just at the border of the present resolution of beam size measurements in the SLC.

All static alignment tolerances are caused by an increase of the vertical beam size, compared with which the effects of induced aberrations on the horizontal beam size (a factor 5 to 6 larger) are always unimportant.

3 Quadrupole Alignment

3.1 Dispersive Kicks

The residual effect of a quadrupole misalignment after orbit correction can be represented by a *dispersive kick*. To see this, we note that the perturbative Hamiltonian of a quadrupole horizontally displaced by a distance X is given by

$$H_{\rm pert} = -\frac{K_q}{2}\ \delta(x_q - X)^2 - K_q X x_q\ , \tag{3.11}$$

where K_q denotes the strength of the quadrupole and x_q is the horizontal coordinate at the center of the magnet. The first part of the Hamiltonian (3.11) contains a chromatic and a dispersion-like term, while the second part represents a closed-orbit distortion. In the case of beam-based alignment, the orbit is steered through the center of each quadrupole. A closed orbit bump which would achieve this is described by the similarity transformation

$$\begin{aligned} &\exp\left\{-p_{xq}X(1-\delta) + x_q\theta(1-\delta)\right\}\ \ \exp\left\{\frac{K_q}{2}\ \delta(x_q - X)^2 + K_q X x_q\right\} \qquad (3.12) \\ &\times \exp\left\{p_{xq}x(1-\delta) - x_q\theta(1-\delta)\right\}\ =\ \exp\left\{\frac{K_q}{2}\ \delta x_q^2 - K_q X\delta^2 x_q + K_q X x_q\right\}\ . \end{aligned}$$

where θ represents the bump angle at the quadrupole and we have dropped terms which do not depend on x_q, since they do not affect the particle trajectories. The resulting Hamiltonian consists of a chromatic term (which is independent of the displacement), a second-order dispersion, and the closed-orbit distortion. In practice, we remove the closed-orbit distortion by means of another corrector, $\exp\{-K_q X x_q(1-\delta)\}$, which leads to the final transformation [12]

$$\begin{aligned} &\exp\left\{\frac{K_q}{2}\ \delta x_q^2 - K_q X \delta^2 x_q + K_q X x_q\right\}\ \exp\left\{-K_q X (1-\delta)\, x_q\right\} \\ &= \exp\left\{\frac{K_q}{2}\ \delta x_q^2 - K_q X \delta^2 x_q + K_q X \delta x_q\right\}\ . \end{aligned} \tag{3.13}$$

Hence, after optimum orbit correction, the displacement X gives rise to a first- and a second-order horizontal dispersion. The latter can be neglected, compared with the first-order contribution. Vertical misalignment is treated analogously. The effect of displacing a quadrupole by X and Y horizontally and vertically, respectively, is then to a very good approximation described by a dispersive kick:

$$\begin{aligned} \Delta p_{xq} &= K_q\, X \delta \\ \Delta p_{yq} &= -K_q\, Y \delta\ . \end{aligned} \tag{3.14}$$

3.2 Maximum Correctable Dispersion

The dispersive kicks, Eq. (3.14), induced by displaced quadrupoles give rise to a finite value of the dispersion at the IP. To correct the horizontal and vertical dispersion at the IP, a $-I$ pair of quadrupoles and skew quadrupoles, respectively, in the CCS is used. The two magnets in each pair are excited equally with opposite sign. The maximum value of dispersion that can be corrected is limited by third-order aberrations generated by these two magnet pairs, and translates into an alignment tolerance for all other quadrupole magnets. The third-order terms are caused by the interaction of the two dispersion-correcting quadrupoles (or skew quadrupoles) with the CCS–sextupoles.

For the horizontal dispersion, the relevant Lie operators read

$$\exp\left\{-H_{q1}(x_{q1}, y_{q1}, \delta)\right\}\ \exp\left\{-H_{s1}(x_{s1}, y_{s1}, \delta)\right\}\ \exp\left\{-H_{s2}(x_{s2}, y_{s2}, \delta)\right\}$$
$$\times \exp\left\{-H_{q2}(x_{q2}, y_{q2}, \delta)\right\}\ \exp\left\{-H_{s3}(x_{s3}, y_{s3}, \delta)\right\}\ , \tag{3.15}$$

where the subindices $q1, q2$ refer to the two magnets of the normal quadrupole pair, and $s1$, $s2$, $s3$ denote the last three sextupoles, as before. If we suppose that the dispersion to be cancelled is generated downstream of the CCS, the first sextupole $s0$ can be ignored. The Hamiltonians of the quadrupoles and sextupoles are given by

$$H_{qi} \approx \frac{K_{qi}}{2} \left\{(x_{qi} + \eta_{qi}\delta)^2 - y_{qi}^2\right\}\ , \tag{3.16}$$
$$H_{si} \approx \frac{K_{si}}{6} \left\{(x_{si} + \eta_{si}\delta]^3 - 3(x_{si} + \eta_{si}\delta)y_{si}^2\right\}\ . \tag{3.17}$$

Thanks to the $-I$-separation in the unperturbed linear optics, we have $x_{q1} = -x_{q2}$ and $y_{q1} = -y_{q2}$. As a consequence, we can easily combine the exponents in Eq. (3.15) to a single Hamiltonian using similarity transformations [6]. Under our assumption that the dispersion to be cancelled is generated downstream of the CCS, we have to propagate the dispersion terms to the right, and thus arrive at

$$\begin{aligned} H_{\mathrm{tot}} \approx\ & H_{s1}\left\{x_{s1} - K_{q1}(x_{q1} + \eta_{q1}\delta)R_{12,q1s1},\ y_{s1} + K_{q1}y_{q1}R_{34,q1s1},\ \delta\right\} \\ +\ & H_{s2}\left\{x_{s2} - K_{q1}(x_{q1} + \eta_{q1}\delta)R_{12,q1s2},\ y_{s2} + K_{q1}y_{q1}R_{34,q1s2},\ \delta\right\} \\ +\ & H_{s3}\left\{x_{s3} - 2K_{q1}\eta_{q1}\delta R_{12,q1s3},\ y_{s3},\ \delta\right\}\ , \end{aligned} \tag{3.18}$$

where use has been made of $\eta_{q1} = \eta_{q2}$, and $R_{12,q1s1}$ denotes the (1,2) R–matrix element from $q1$ to $s1$, etc. In this Hamiltonian, we have explicitly taken into account the dispersion, so that the transformation to IP coordinates $(x_0, p_{x0}, y_0, p_{y0})$ has to be performed via the 4×4 R–matrices (and not by the 6×6 R–matrices, which will be used in some of the later paragraphs). From Eq. (3.18), and assuming a typical momentum spread $\delta = 3 \times 10^{-3}$, the most important induced third-order aberrations are identified as the $p_{y0}^2\delta$ and the $p_{y0}^2 p_{x0}$ terms. Both terms contribute about equally to the final beam size. The $p_{y0}^2\delta$ contribution can, in principle, be corrected, but destroys the orthogonality of chromaticity and dispersion correction, while the $p_{x0}p_{y0}^2$ coefficient cannot be corrected at all, in the present SLC final focus. The maximum tolerable value of K_{q1} due to these terms is about 5×10^{-4} m^{-1}, corresponding to a horizontal dispersion

$$|\eta_{x0,\mathrm{max}}| \approx 0.7\,\mathrm{mm}\ . \tag{3.19}$$

The correction of the vertical dispersion is performed by use of the skew quadrupole pair. Equation (3.15) also applies in this case, if we replace the Hamiltonian H_{qi} by H_{sqi},

$$H_{sqi} \approx -K_{sqi}(x_{sqi} + \eta_{sqi}\delta)\ y_{sqi}\ . \tag{3.20}$$

Again assuming that the (vertical) dispersion to be corrected is induced downstream of the CCS, the resulting total Hamiltonian is

$$\begin{aligned} H_{\mathrm{tot}} \quad &\approx \quad H_{s1}\left\{x_{s1} + K_{sq1}y_{sq1}R_{12,sq1s1},\ y_{s1} + K_{sq1}(x_{sq1} + \eta_{sq1}\delta)\ R_{34,sq1s1},\ \delta\right\} \\ &\times \quad H_{s2}\left\{x_{s2} + K_{sq1}y_{sq1}R_{12,sq1s2},\ y_{s2} + K_{sq1}(x_{sq1} + \eta_{sq1}\delta)K_{34,sq1s2},\ \delta\right\} \\ &+ \quad H_{s3}\left\{x_{s3},\ y_{s3} + 2K_{sq1}\eta_{sq1}\delta R_{34,sq1s3},\ \delta\right\}\ . \end{aligned} \tag{3.21}$$

After transforming to the IP, the two dominant beam-size increasing aberrations are the $p_{y0}\delta^2$ and $p_{x0}p_{y0}\delta$ terms, which give a maximum value for the integrated skew-quadrupole strength K_{sq1} of about 10^{-3} m^{-1}. This amounts to a maximum correctable dispersion of

$$|\eta_{y0,\max}| \approx 0.62 \text{ mm} , \tag{3.22}$$

which is similar to the horizontal value. The treatment of upstream-dispersion correction is completely analogous, and results in about the same value of correctable dispersion.

Tracking simulations have been performed using MAD [5] for comparison and verification of the analytical estimate. In these simulations, a dispersive kick, Eq. (3.14), was applied at the center of a selected quadrupole magnet in a model of the SLC final focus. After subsequent dispersion correction, 10,000 particles were tracked through this model. From the observed increase of the vertical rms beam size at the IP as a function of the dispersive kick strength, a maximum displacement of the quadrupole magnet could be deduced. The maximum displacement of several magnets was found for $|\eta_{x,y,\max}| \approx 0.65$ mm, in satisfactory agreement with Eqs. (3.19) and (3.22). However, for almost all magnets in the upper transformer, considerably larger beam-size increases were obtained than could be explained by the dispersion generated at the IP. The tolerances for these magnets are, in fact, not given by the value of $\eta_{x0,y0}$, but instead by the value of the slope of the dispersion $\eta'_{x0,y0}$, which may interact with other aberrations in the final focus. This interaction is the subject of the next section.

3.3 Interaction of Dispersion and Higher Order Aberrations

The residual aberrations in the 1994 final focus are mainly due to the interaction of the interleaved sextupoles with each other, while to some extent they are also due to the long sextupole effect [6], and the interaction of the sextupoles with the triplet and with other quadrupole magnets. Values for the coefficients of these higher order terms have been obtained by a detailed analysis [13, 14]. They are listed in Table 1.

Monomial	Coefficient [m]	$(\Delta\sigma_y^2)^{1/2}$ [nm]
Linear	—	290
$p_{x0}\, p_{y0}^2\, \delta$	-847	272
$p_{x0}^2\, p_{y0}^2$	-3124	153
p_{y0}^4	646	91
$p_{y0}^2\, \delta^2$	5	29

Table 1: Remaining aberrations in the 1994 SLC final focus [14] and their respective contribution to the vertical spot size.

The SLC final focus can be approximately represented as

$$\exp\left\{-a\, p_{y0}^4 - b\, p_{x0}\, p_{y0}^2\, \delta - c\, p_{y0}^2\, p_{x0}^2\right\} , \tag{3.23}$$

where $a \approx 646$ m, $b \approx -847$ m, and $c \approx -3124$ m, and the variables p_{x0} and p_{y0} are the transverse momenta at the IP. A dispersive kick, $\exp\{x_0 \eta'_{x0} \delta\}$, applied somewhere in the upper transformer will interact with the aberrations in Eq. (3.23), resulting in

$$\begin{aligned} &\exp\{x_0 \eta'_{x0}\delta\}\ \exp\left\{-a\, p_{y0}^4 - b\, p_{x0} p_{y0}^2 \delta - c\, p_{y0}^2\, p_{x0}^2\right\} \qquad (3.24) \\ &= \exp\left\{-a\, p_{y0}^4 - b\, (p_{x0} + \eta'_{x0}\delta)\, p_{y0}^2 \delta - c\, p_{y0}^2\, (p_{x0} + \eta'_{x0}\delta)^2\right\}\ \exp\{x_0 \eta'_{x0}\delta\}\ . \end{aligned}$$

Here a similarity transformation, Eq. (1.4), has been performed. Notice that the factor $\exp\{x_0 \eta'_{x0} \delta\}$, i.e., the second operator, does not affect the vertical beam size since $[x_0, y_0] = 0$. The total Hamiltonian of the first Lie operator is

$$H_{\rm tot} = a\, p_{y0}^4 + p_{x0}\, p_{y0}^2\, \delta (b + 2c\, \eta'_{x0}) + c\, p_{y0}^2\, p_{x0}^2 + (b\, \eta'_{x0} + c\, \eta'^2_{x0})\, p_{y0}^2\, \delta^2 \ . \quad (3.25)$$

This Hamiltonian allows the following conclusions:

1. The terms depending on η'_{x0} will cause an alignment tolerance for the magnets in the upper transformer.
2. It is evident that by proper choice of η'_{x0}, the dominant remaining aberration $p_{y0}^2\, p_{x0}\, \delta$ may partly be cancelled, at the expense of generating a $p_{y0}^2\, \delta^2$ term—the very term that the upgrade was designed to cancel. There will be an optimum value of η'_{x0}, as generated at the start of the final focus, which will yield a minimum spot size.
3. The Hamiltonian is asymmetric with respect to η'_{x0}, meaning that for zero incoming slope of dispersion, the alignment tolerances will be much tighter for displacements in one direction than in the other.

Figure 1 shows the vertical beam size as a function of η'_{x0}. The analytical prediction obtained from the Hamiltonian (3.25) and the result of tracking 10,000 particles (dots) agree quite well, and confirm all three of the above statements. The small discrepancy between the analytical curve and the simulation is partly explained by the statistical error of the tracking, and is partly due to a slightly different representation of magnets.

In the following, we assume that the incoming dispersion is somehow adjusted close to its optimum value ($\eta'_{x0} \approx -19$ mrad) and calculate all

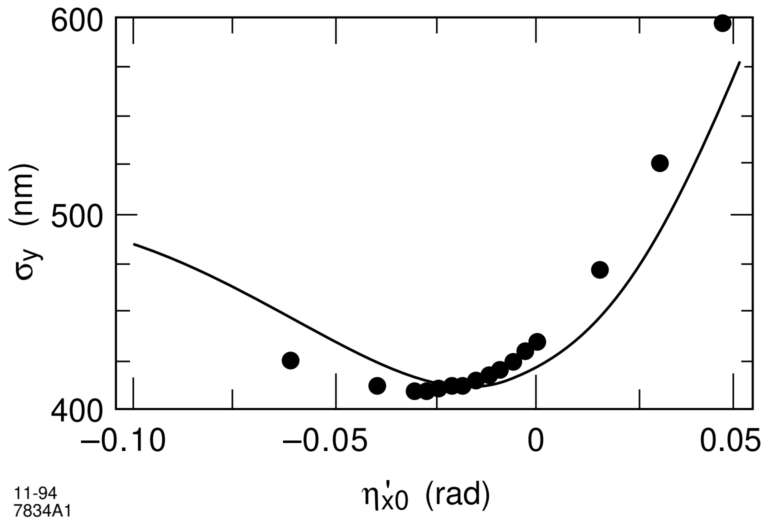

Figure 1: Vertical beam size σ_y in nanometers as a function of the slope of the incoming horizontal dispersion η'_{x0} (value propagated to the IP), according to the analytical estimate (3.25) (curve), and as obtained by multiparticle tracking (dots).

tolerances with respect to this point. From Fig. 1, the tolerance on the horizontal slope of dispersion is about

$$|\eta'_{x0,\max}| \approx 13 \text{ mrad} . \tag{3.26}$$

This value determines the horizontal alignment tolerance of quadrupoles in the upper transformer.

Figure 2(a) illustrates the improvement of the vertical spot size that can be achieved by optimizing the incoming slope of dispersion, as a function of momentum spread. In Fig. 2(b), the optimum value of η'_{x0} is depicted. Overall, the spot size can be reduced by about 5% by proper tuning of the horizontal dispersion. The results suggest a regular monitoring of the dispersion in the upper transformer. The asymmetry of $\sigma_{y0}(\eta'_{x0})$ in Fig. 1 disappears when octupole magnets are installed in a future upgrade, which will cancel the $p_{y0}^2\, p_{x0}\, \delta$ term in the Hamiltonian of Eq. (3.23) [4].

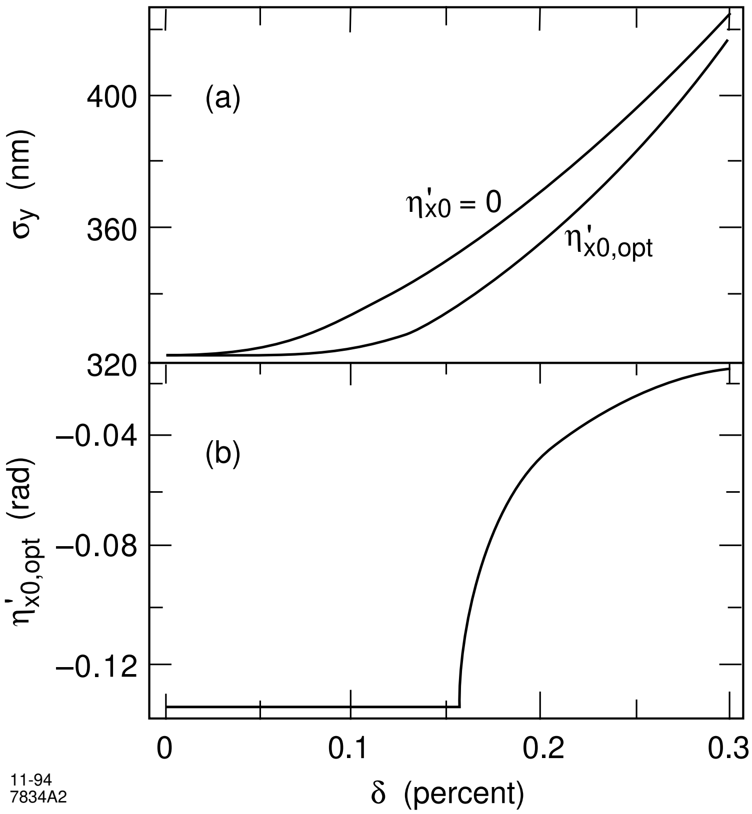

Figure 2: Effect of nonzero slope of horizontal dispersion, generated upstream of the CCS, as a function of momentum spread; (a) optimum vertical beam size compared with the case $\eta'_{x0} = 0$; (b) optimum value of η'_{x0}.

Incoming vertical dispersion is treated similarly to the horizontal case. The product of Lie operators now reads

$$\exp\left\{y_0\,\eta'_{y0}\,\delta\right\}\ \exp\left\{-a\,p_{y0}^4 - b\,p_{x0}\,p_{y0}^2\,\delta - c\,p_{y0}^2\,p_{x0}^2\right\}\ , \tag{3.27}$$

yielding

$$\begin{aligned} H_{\text{tot}} \quad &= \quad a\,p_{y0}^4 + 4a\,\eta'_{y0}\,p_{y0}^3\,\delta + 6a\,\eta_{y0}^{\prime 2}\,p_{y0}^2\,\delta^2 + 4a\,\eta_{y0}^{\prime 3}\,p_{y0}\,\delta^3 \\ &+ \quad b\,p_{y0}^2\,p_{x0}\delta + b\,\eta'_{y0}\,p_{y0}\,p_{x0}\,\delta^2 + b\,\eta_{y0}^{\prime 2}\,p_{x0}\,\delta^3 \\ &+ \quad c\,p_{y0}^2\,p_{x0}^2 + 2c\,\eta'_{y0}\,p_{y0}\,p_{x0}^2\,\delta + c\,p_{y0}^2\,p_{x0}^2\ . \end{aligned} \tag{3.28}$$

From this Hamiltonian, the vertical beam size increase due to an incoming slope of the vertical dispersion η'_{y0} can be deduced. This is shown in Fig. 3, together with the results of multiparticle tracking. No significant asymmetry is observed, so that $\eta'_{y0} \approx 0$ is the best choice. The vertical slope of dispersion gives rise to the vertical alignment tolerance of the upper transformer magnets. According to Fig. 3, this is given by

$$|\eta'_{y0,UT,\max}| \approx 13 \text{ mrad} , \tag{3.29}$$

which is the same value as for the horizontal dispersion.

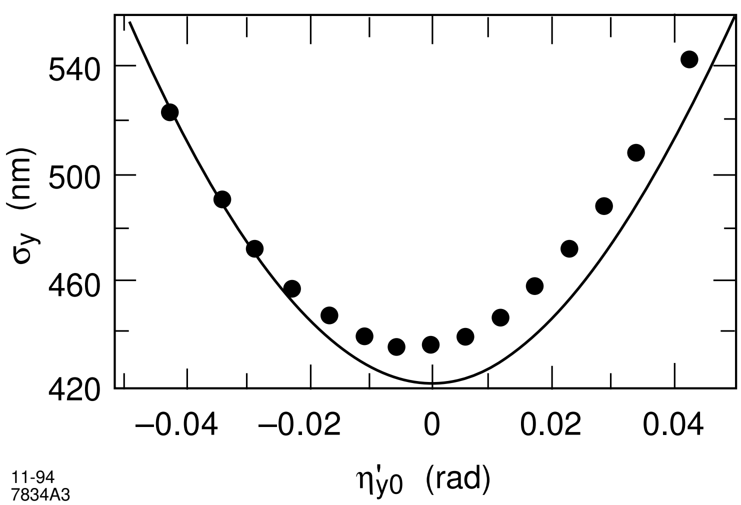

Figure 3: Vertical beam size σ_y in nanometers as a function of the slope of the incoming vertical dispersion η'_{y0} (value propagated to the IP), according to the analytical estimate (curve), Eq. (3.28), and as obtained by multiparticle tracking (dots).

3.4 Dispersion and Triplet Chromaticity

Tracking studies have revealed that still another effect is responsible for the vertical alignment tolerance of several magnets in the final transformer and in the CCS: the interaction of $\exp\{\eta'_{y0}\, y_0\, \delta\}$ with the uncompensated triplet chromaticity that gives rise to second-order vertical dispersion. The vertical chromatic aberration of one of the final quadrupoles can be written

$$\exp\left\{-c_1\, \delta\, y_q^2 - c_2\, \delta\, p_{yq}^2\right\} \ , \tag{3.30}$$

where the y_q, p_{yq} are the coordinates at the center of the quadrupole. The coefficients c_1 and c_2 for a thick quadrupole of length L_q are given by [6]

$$c_1 \ = \ \begin{cases} \frac{1}{4}\, K_q \left[1 + \left(\sinh\sqrt{K_q L_q} \Big/ \sqrt{K_q L_q}\ \right)\right], \ \text{if} \ \ K_q > 0 \ , \\ \\ \frac{1}{4}\, K_q \left[1 + \left(\sin\sqrt{|K_q| L_q} \Big/ \sqrt{|K_q| L_q}\ \right)\right], \ \text{if} \ \ K_q < 0 \ , \end{cases} \tag{3.31}$$

$$c_2 \ = \ \begin{cases} -\frac{1}{4}\, L_q \left[1 - \left(\sinh\sqrt{K_q L_q} \Big/ \sqrt{K_q L_q}\ \right)\right], \ \text{if} \ K_q > 0 \ , \\ \\ -\frac{1}{4}\, L_q \left[1 - \left(\sin\sqrt{|K_q| L_q} \Big/ \sqrt{|K_q| L_q}\ \right)\right], \ \text{if} \ K_q < 0 \ . \end{cases} \tag{3.32}$$

The Hamiltonian arising from the interaction with the incoming vertical dispersion η'_{y0} reads

$$H_{\text{tot}} \ = \ -2c_1\, \eta'_{y0}\, \delta^2\, y_q\, R_{34,q0} + 2c_2\, \eta'_{y0}\, \delta^2\, p_{yq}\, R_{33,q0} \ . \tag{3.33}$$

After transforming y_q and p_{yq} to the IP, the spot size can be evaluated as a function of η'_{y0}. The result is shown in Fig. 4, from which a maximum value for η'_{y0} of about 0.51 mrad is expected. In the tracking, a 2% beam size increase was found for $\eta'_{y0} \approx 0.52$ mrad and $\eta'_{y0} \approx -1.05$ mrad, respectively. The dispersion was generated in the final transformer upstream of the triplet. We have chosen

$$|\eta'_{y0,FT,\max}| \ \approx \ 0.8 \text{ mrad} \tag{3.34}$$

as our tolerance. The same interaction occurs for dispersion generated inside the CCS. For these magnets, however, about half the chromaticity of the

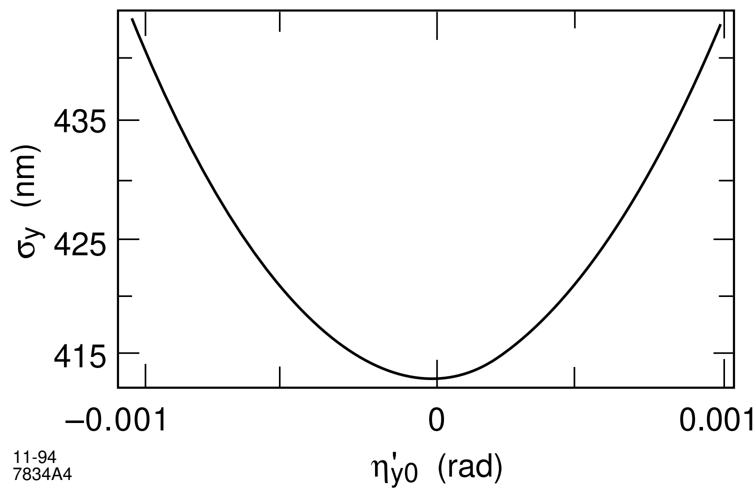

Figure 4: Vertical beam size as a function of the slope of vertical dispersion, generated between the CCS and the final triplet.

final triplet is corrected, so that the tolerance is loosened by about a factor of 2, and we therefore assume

$$|\eta'_{y0,CCS,\max}| \approx 1.6 \text{ mrad} . \tag{3.35}$$

This tolerance was also confirmed by tracking.

3.5 Summary of Quadrupole Alignment Tolerances

In the previous sections, the maximum correctable dispersion and the maximum tolerable slope of dispersion at the IP due to a quadrupole displacement were calculated . The results are summarized by

$$|\eta_{x0}| < 0.65 \text{ mm, for all magnets} , \tag{3.36}$$

$$|\eta_{y0}| < 0.65 \text{ mm, for all magnets} , \tag{3.37}$$

$$|\eta'_{x0}| < 13 \text{ mrad, for all magnets} , \tag{3.38}$$

$$|\eta'_{y0}| < \begin{cases} 13 \text{ mrad, for UT magnets} , \\ 1.6 \text{ mrad, for CCS magnets} , \\ 0.8 \text{ mrad, for FT magnets} . \end{cases} \tag{3.39}$$

Strictly speaking, the tolerance due to η'_{x0} only applies to magnets in the UT. Extending it to all quadrupoles is thus very conservative. However, the maximum value of η'_{x0} does not affect the total horizontal alignment tolerance for any magnet outside the UT. It should be pointed out that the tolerances for magnets in the UT may be looser than quoted, since the dispersion generated in front of the CCS can, in principle, be corrected by means of two quadrupoles and two skew quadrupoles located at the entrance of the final focus system [15].

The horizontal and vertical alignment tolerances of the quadrupole magnets are each determined by two terms in the Hamiltonian (dispersion and slope of dispersion at the IP). In almost all cases, the two limitations imposed by η and η' differ by at least an order of magnitude, either in one direction or the other. We take the maximum displacement allowed by the tighter of these two terms as the final alignment tolerance for a specific magnet.

The alignment tolerances for almost all magnets in the UT are due to the interaction of $\eta'_{x0,y0}$ with the residual aberrations of the final focus. Interaction with the triplet chromaticity is responsible for the vertical alignment tolerance of some magnets in the CCS and in the FT, for which the R_{34} matrix element to the triplet is significant. All other tolerances are caused by the maximum dispersion at the IP that can be corrected.

Even though the sources of the tolerances are quite different, the actual values are about the same, with the tightest tolerances being in the order of 100 μm for all three cases. It should be noted that we have attributed equal weight to all magnets, and that the tightest tolerances may be slightly loosened at the expense of reducing the other ones.

To verify the applicability of the derived alignment tolerances, multi-particle tracking studies were performed for different random seeds of magnet displacements and subsequent orbit correction. If our tolerance conditions are met, the expected beam size increase is smaller than 4–8%. This was confirmed in the simulation studies.

4 Sextupole Alignment

4.1 Bump Amplitudes

Horizontal and vertical orbit bumps can be used to steer through the center of misplaced sextupole magnets. In actual SLC operation, symmetric and antisymmetric displacements of the two sextupole pairs are measured and corrected with orbit bumps through the sextupoles [16]. The following analysis is based on a particular set of orbit bumps where those corrector magnets closest to the sextupole have been chosen for generating a bump through the center of a misaligned sextupole under the further restriction that the bump amplitude is zero in the other three sextupoles.

When a bump is used to steer the beam through the center of a misaligned sextupole, as a byproduct, the beam is steered off-center through the (ideally aligned) quadrupoles. This generates the same dispersion as that caused by a quadrupole displacement. Since the orbit bump typically extends over several quadrupole magnets, the contributions from these quadrupoles to the IP dispersion (or slope of IP dispersion) add or cancel each other, depending on the R-matrices between them, and on the sign and amplitude of the bump at each quadrupole.

A simulation study has been performed according to the following recipe: The orbit is steered through the center of a displaced sextupole by a closed bump. The values of the displacements X and Y chosen correspond to a beam size increase by 2%, as calculated from the displacements in the quadrupoles alone, by evaluating the coherent contributions to $\eta_{x0,y0}$ and $\eta'_{x0,y0}$ separately, and adding their effect in quadrature. The dispersion at the IP has then been corrected and, for a few cases, the vertical chromaticity due to the interaction of the horizontal bump and the sextupole has also been compensated. The beam size obtained in the tracking agrees well with expectations, even though no attempt at further optimization and tuning has been made. This confirms that the maximum bump amplitude is solely caused by the generated orbit offsets in the quadrupole magnets, and is not affected by the sextupole Hamiltonians. As an exception, a 20% increase of the beam size for one particular orbit bump is due to the chromatic skew quadrupole induced by the bump-sextupole interaction, which cannot easily be corrected.

4.2 Orthogonality

If the beam is too much off center in the sextupole magnets, the orthogonal control of chromaticity and waist motion is destroyed. This leads to an upper bound on the allowable orbit offset in the sextupoles. We somewhat arbitrarily require that for chromaticity changes corresponding to a beam size increase by a factor $\sqrt{3}$, the contribution from all other aberrations (except chromaticity) caused by a horizontal or vertical offset in the sextupole is less than 10% of the total beam size [17]. This criterion translates into

$$(\Delta\sigma^2_{x,y})^{\frac{1}{2}} \;<\; 0.8\,\sigma_{x0,y0}\;. \tag{4.40}$$

In this case, the term $\sigma_{x0,y0}$ denotes the optimum design beam size, and $(\Delta\sigma^2_{x,y})^{\frac{1}{2}}$ is the additional increase (due to terms other than chromaticity) that accompanies the chromatic change of the beam size by a factor of $\sqrt{3}$. The vertical chromaticity scan sets a tolerance for the Y-sextupoles $s1$ and $s3$, while the limit for the X-sextupoles $s0$ and $s2$ is imposed by the horizontal chromaticity scan.

Changing the strength of an off-center sextupole by ΔK_s gives rise to the perturbative Hamiltonian

$$\begin{aligned} H_{\rm pert} \;&=\; -\frac{1}{2}\,\Delta K_s\;X(x^2-y^2)\;+\;\frac{1}{2}\,\Delta K_s\;X^2x \\ &\quad -\frac{1}{2}\,\Delta K_s\;Y^2y+\Delta K_sYxy\;, \end{aligned} \tag{4.41}$$

where X and Y denote the displacement between sextupole and beam orbit. The terms in this Hamiltonian can readily be identified as quadrupole, horizontal and vertical kick, and skew quadrupole. The Hamiltonian (4.41) does not explicitly contain dispersion and δ-dependence, so that the transformation to IP coordinates has to be performed via the inverse 6×6 instead of the 4×4 R–matrices. The resulting increase of the vertical beam size is obtained from

$$\begin{aligned} \Delta\sigma_y^2 \;&\approx\; (\Delta K_s)^2\;X^2\theta_{y0}^2\;R^{-1\;4}_{34,s0} \\ &+\; (\Delta K_s)^2\;Y^2\theta_{x0}^2\;R^{-1\;2}_{12,s0}R^{-1\;2}_{34,s0} \\ &+\; (\Delta K_s)^2\;Y^2\;\delta^2\;R^{-1\;2}_{16,s0}\;R^{-1\;2}_{34,s0}\;. \end{aligned} \tag{4.42}$$

The tolerances for $s1$ and $s3$ are deduced from this equation. A similar expression applies to the horizontal case, which limits the other two sextupoles.

4.3 Interaction with other Sextupoles

A second limitation on the tolerable orbit offset in a sextupole arises directly from the additional aberrations introduced from destruction of the $-I$ and from the resultant spot size increase. If the orbit in a sextupole 'si' is horizontally off center by a distance X, the perturbative Hamiltonian is an additional quadrupole at the position of the sextupole

$$H_{\mathrm{pert},X} \approx -\frac{1}{2}\, K_{si}\, X(x_{si}^2 - y_{si}^2)\ . \tag{4.43}$$

This quadrupole may destroy the π phase advance between the sextupole pairs, causing an alignment tolerance (specifically, how well the orbit bump must be adjusted to the center of the magnet). This effect is important only for the two inner sextupoles, since correction further upstream or downstream can easily compensate for a quadrupole-like term at $s0$ or $s3$. The interaction of the Hamiltonian (4.43) with another sextupole 'sj', gives

$$H_{\mathrm{pert},X,ij} \approx -\frac{1}{2}\, K_{si}\, K_{sj}\, X(R_{12,ij}\, x_{si} x_{sj}^2 - R_{12,ij}\, x_{si} y_{sj}^2 + 2R_{34,ij}\, y_{si}\, x_{sj}\, y_{sj})\ , \tag{4.44}$$

where we assume $i < j$. After transformation to IP coordinates by means of the inverse 6×6 R–matrices, the Hamiltonian (4.44) contains monomials of the form $p_{x0}\, p_{y0}^2$ and $\delta\, p_{y0}^2$, which will affect the vertical spot size. The second of these terms is identified as vertical chromaticity which can be tuned out. The horizontal displacement tolerance is thus determined by the induced geometric term $p_{x0}\, p_{y0}^2$ alone.

For a vertical offset Y at the ith sextupole, the perturbative Hamiltonian is a skew quadrupole

$$H_{\mathrm{pert},Y} \;\approx\; \frac{1}{2}\, K_{si}\; Y(2x_{si}y_{si}) \;. \tag{4.45}$$

The treatment proceeds in analogy to the horizontal case, and the Hamiltonian due to an interaction with the jth sextupole is

$$H_{\mathrm{pert},Y,ij} \;\approx\; \frac{1}{2}\, K_{si}\, K_{sj}\;\; Y(R_{12,ij}\, y_{si}\, x_{sj}^2 - R_{12,ij}\, y_{si}\, y_{sj}^2 - 2R_{34,ij}\, x_{si}\, x_{sj}y_{sj}) \;, \tag{4.46}$$

where again $i < j$ is assumed. Transforming to IP coordinates reveals four relevant monomials, namely $p_{y0}\, p_{x0}^2$, p_{y0}^3, $p_{y0}\, p_{x0}\, \delta$, and $p_{y0}\, \delta^2$. The first two are purely geometric aberrations, the third is a chromatic skew quadrupole, and the last corresponds to second-order dispersion. None of these can easily be corrected, and they all contribute to the vertical tolerance.

4.4 Summary of Sextupole Alignment Tolerances

The maximum amplitude of the orbit bumps used to steer through the center of a misaligned sextupole varies between a few millimeters horizontally and values as low as 100–200 μm for the vertical bumps at $s2$ and $s3$. However, another selection of corrector magnets may well lead to improved tolerance limits. The maximum bump amplitudes are always imposed by the displacement inside the quadrupoles and the resulting dispersion. These amplitude values are a measure of the required absolute magnet alignment.

The second tolerance calculated is related to the accuracy to which the beam orbit has to be steered through the center of the sextupoles. It specifies how well the magnets have to be positioned (in case of beam-based alignment), and the quality and stability of the orbit bumps and the beam orbit. Two different contributions give rise to this tolerance: the destruction of the $-I$ between sextupole pairs, and the orthogonality criterion. The relative alignment tolerances for $s0$ and $s3$ are due to the orthogonal tuning condition, and have typical values of a few hundred microns. The alignment tolerances for the inner two sextupoles are, however, solely due to the additional aberrations. For these two magnets, the horizontal alignment has to be of the order of 100 μm, while the vertical is even tighter (50–70 μm).

5 Conclusions

Lie algebra techniques were used to evaluate alignment tolerances for all quadrupole and sextupole magnets in the 1994 SLC final focus. The analytically calculated numbers were confirmed by multiparticle tracking.

Special attention should be paid to certain magnets with very tight tolerances: the horizontal and vertical alignment tolerance of the final triplet, as well as the vertical alignment tolerances of some quadrupoles in the final transformer, the CCS, and the upper transformer are all only of the order of 100 μm. This is remarkable in so far as these tolerances are due to three completely different effects (maximum correctable dispersion, interaction with the triplet chromaticity, and interaction with the remaining aberrations of the final focus system, respectively). Furthermore, our analysis suggests it is necessary to control the incoming slope of the horizontal dispersion, which, if mismatched, could easily cause significant spot size increases.

While it seems possible to use orbit bumps to adjust the orbit in misaligned sextupoles up to amplitudes between a few hundred microns or even several millimeters, the tolerance of these bumps is rather tight for the two inner sextupoles: the adjustment has to be as good as 100 μm horizontally, and about 50–70 μm vertically. The latter is, presumably, the tightest tolerance in the final focus, apart from the unlikely displacement of the final triplet quadrupoles with respect to each other.

In 1994, all quadrupoles and sextupoles of the SLC final focus were aligned to the specified tolerances using beam-based procedures. The fact that in the system so aligned, the design spot size could easily be achieved, testifies to the validity of the calculations.

Finally, we point out that Lie algebra methods are an elegant tool for analyzing nonlinear aberrations and limitations in final focus systems—they allow a clear understanding of how different perturbations interact with each other. In particular, similarity transformations are well suited for many applications. Multiparticle tracking is, however, still a useful supplement, since it can confirm the Lie algebra analysis, and thus ensure that all important effects have been included in the Hamiltonians considered. Conversely, as demonstrated, Lie algebra techniques may help to understand tracking results.

Acknowledgements

The author thanks N. Walker for encouragement and many stimulating discussions. P. Emma, J. Irwin, and M. Woodley deserve his thanks for various useful suggestions. Furthermore, he is grateful to T. Raubenheimer for help in installing and using MAD.

References

[1] K. L. Brown, "A Conceptual Design of Final Focus Systems for Linear Colliders," in the Proceedings of the US–CERN Joint Topical Course, Frontiers of Particle Beams, South Padre Island, Texas, 1986, and SLAC preprint SLAC–PUB–4159 (1987).

[2] J. J. Murray, K. L. Brown, and T. Fieguth, "The Completed Design of the SLC Final Focus System," in *Proc. of PAC 87,* Washington, D.C., 1987, and SLAC preprint SLAC–PUB–4219 (1987).

[3] *SLC Design Handbook*, Chap. 4, 1984.

[4] N. Walker, R. Helm, J. Irwin, and M. Woodley, "Third-Order Corrections to the SLC Final Focus," in *Proc. of PAC 93,* Washington, D.C., 1993, and SLAC preprint SLAC–PUB–6206 (1993) .

[5] H. Grote and F. C. Iselin, *The MAD Program, Version 8.1, User's Reference Manual,* CERN Report CERN/SL/90–13 (AP) (1990).

[6] J. Irwin, "The Application of Lie Algebra Techniques to Beam Transport Design," Nucl. Instrum. Methods **A298**, 460 (1990), and SLAC preprint SLAC–PUB–5315 (1990).

[7] K. L. Brown, *A First– and Second–Order Matrix Theory for the Design of Beam Transport Systems and Charged Particle Spectrometers,* SLAC Report SLAC–75 (1982); K. L. Brown and R. Servranckx, "First and Second Order Charged Particle Optics," in the Proceedings of the 3rd Summer School on High Energy Particle Accelerators, Upton, New York, 1983, and SLAC preprint SLAC–PUB–3381 (1983).

[8] K. Brown, F. Rothacker, D. Carey, and C. Iselin, *TRANSPORT—A Computer Program for Designing Charged Particle Beam Transport Systems,* SLAC Report SLAC–91 (1977).

[9] P. Chen, "Disruption Effects from the Collision of Quasi-Flat Beams," SLAC preprint SLAC–PUB–6215 (1993).

[10] G. Roy and J. Irwin, "Next-Generation Linear Collider Final Focus System Stability Tolerances," SLAC preprint SLAC–PUB–5652 (1991).

[11] G. Roy, *Analysis of the Optics of the Final Focus Test Beam Using Lie Algebra Based Techniques,* SLAC Report SLAC–397 (1992).

[12] N. Walker, private discussion, 1993.

[13] N. Walker, J. Irwin, and M. Woodley, "Analysis of Higher-Order Optical Aberrations in the SLC Final Focus using Lie Algebra Techniques," in *Proc. of PAC 93,* Washington, D.C., 1993, and SLAC preprint SLAC–PUB–6205 (1993).

[14] N. Walker, private communication, 1993.

[15] P. Emma, private communication, 1994.

[16] P. Emma, J. Irwin, N. Phinney, P. Raimondi, N. Toge, N. Walker, and V. Ziemann, "Beam Based Alignment of the SLC Final Focus Sextupoles," in *Proc. of PAC 93,* Washington, D.C., 1993, and SLAC preprint SLAC–PUB–6209 (1993).

[17] N. Walker, private communication, 1993.